Journal of Nuclear Medicine, published on June 8, 2017 as doi:10.2967/jnumed.116.182170

Noninvasive Interrogation of Cancer Metabolism with Hyperpolarized ^{13}C Magnetic Resonance Imaging

Andrew Cho[1], Justin Y.C. Lau[2,3], Benjamin J. Geraghty[2,3], Charles H. Cunningham[2,3] and Kayvan R. Keshari[1,4,5]

[1]Weill Cornell Medical College, New York NY, USA

[2]Physical Sciences, Sunnybrook Research Institute, Toronto ON, Canada

[3]Department of Medical Biophysics, University of Toronto, Toronto ON, Canada

[4]Department of Radiology, Memorial Sloan Kettering Cancer Center, New York NY, USA

[5]Molecular Pharmacology Program, Memorial Sloan Kettering Cancer Center, New York NY, USA

Corresponding Author:

Kayvan R. Keshari, PhD

Department of Radiology and Molecular Pharmacology Program

Memorial Sloan Kettering Cancer Center

1275 York Avenue, New York NY, 10065, USA.

Email: rahimkk@mskcc.org

Phone: 646-888-3631 Fax: 646-422-0247

First Author:

Andrew Cho

Weill Cornell Medical College, 1300 York Avenue, New York NY, USA. Graduate Student. Email: choa@mskcc.org Phone: 646-888-3650 Fax: 646-422-0247

Word Count: 3491

Running title: Hyperpolarized MRI of Cancer Metabolism

Abstract: This review will highlight recent advances in hyperpolarized ^{13}C magnetic resonance spectroscopic imaging (MRSI), which can be used to non-invasively interrogate tumor metabolism. After providing an overview of magnetic resonance and hyperpolarization, we will discuss the latest advances in data acquisition techniques. Next, we will shift our focus to hyperpolarized probe design and provide an overview of the latest hyperpolarized MRSI probes developed in the last several years.

INTRODUCTION

In the setting of cancer, cellular metabolism is reprogrammed to support proliferation *(1,2)*. Therefore, cancer cells exhibit a unique metabolic fingerprint that provides a means to differentiate them from benign tissues. Over the years, a variety of imaging probes have been developed to non-invasively detect cancer-specific metabolic changes. The most commonly used probe is the positron emission tomography radiotracer 2-^{18}F-fluoro-2-deoxyglucose, which structurally mimics glucose and exhibits increased uptake in malignant cells due to their elevated energetic demand. FDG-PET has been an effective tool for staging and re-staging tumors to determine prognosis and therapeutic response, and it has demonstrated utility in detecting distant metastases *(3)*. However, numerous enzymatic pathways downstream of cellular glucose uptake are also perturbed in cancer (Fig. 1) and assessment of these alterations can provide additional criteria for tumor characterization and patient stratification. In recent years, the emergence of hyperpolarized ^{13}C-MRSI has provided a means to non-invasively quantify flux through enzymatic pathways *in vivo*. This technology is becoming increasingly clinically relevant as a new wave of drugs that target specific metabolic pathways, as opposed to DNA synthesis or repair mechanisms which are the target of traditional

chemotherapy, are entering the Food and Drug Administration approval pipeline *(4,5)*. In recent years, the field of hyperpolarized MRSI has made great strides towards improving data acquisition methods, while other groups in the field have developed an array of probes with the ability to non-invasively measure glycolysis, glutaminolysis, isocitrate dehydrogenase (IDH) activity, pH, and redox status.

MAGNETIC RESONANCE & HYPERPOLARIZATION

MRSI interrogates the magnetic properties of atomic nuclei to acquire an array of spatially resolved nuclear magnetic resonance spectra throughout a volume of interest, such as a patient's body. The resonance frequency of a spectral peak, expressed in parts per million relative to the frequency of a reference standard, is known as its 'chemical shift' and can be used to identify compounds and to quantify metabolite concentrations. With respect to cancer, this information can be used to determine malignancy and for tumor metabolic profiling *(6)*. Furthermore, spectrometers can be tuned to selectively probe certain elements, e.g. carbon, which is the focus of this review. ^{13}C-MRSI is limited by its low sensitivity due the small gyromagnetic ratio and low natural abundance of ^{13}C (1.1%), which is the only stable isotope of carbon that can be detected via magnetic resonance. Thus, it is difficult to acquire high signal-to-noise ratio (SNR) spectra of endogenous metabolites with ^{13}C-MRSI even with multiple scans averaged over long periods of time. To circumvent this limitation, hyperpolarization can be used to facilitate the acquisition of high SNR spectra in under a second.

During MRSI data acquisition, the subject is placed within an external magnetic field. When MR-active nuclei such as ^{13}C are exposed to this field, the magnetic dipole vectors of atomic nuclei align either parallel or anti-parallel with the external field (Fig.

2A) and the number of nuclei in each alignment is dictated by the Boltzmann distribution. The sum of these vectors, also known as ‘spins’, is the net magnetization vector of the sample. Note that each pair of parallel and anti-parallel spins offset each other and there is usually only a small excess of parallel spins. Thus, the sum of the excess parallel spins is equal to the sample net magnetization vector, and the percentage of excess parallel spins relative to the total number of spins in the sample is known as the polarization percentage. The magnitude of the sample magnetization vector is directly proportional to spectral SNR, with larger vectors facilitating high SNR data in shorter acquisition times. At room temperature in a 3 Tesla field, a typical field strength for a clinical grade MRSI scanner, ^{13}C thermal equilibrium polarization is only 2.57 x 10^{-4} %. While thermal equilibrium is the energetically favorable low energy state of the system for a given field strength and temperature, higher polarization values can be reached for short periods of time via hyperpolarization.

For clinical translational applications, hyperpolarization is commonly achieved via dissolution dynamic nuclear polarization *(7)*. The fundamentals of this modality lay in three properties of spin polarization; i) polarization percentage is directly proportional to increasing magnetic field strength and decreasing temperature, ii) electron spins polarize more readily than carbon nuclear spins, iii) spin polarization can be transferred from electrons to ^{13}C nuclei via microwave irradiation *(8)* (Figure 2B). Due to the high-energy irradiation and low temperature required for this technique, dissolution dynamic nuclear polarization must be performed outside of living organisms. Thus, endogenous metabolites within the body cannot be hyperpolarized by this technique, but hyperpolarized compounds can be injected into patients. During polarization, a metabolite of interest is dissolved in a biocompatible solvent in the presence of a free

radical-containing compound. The solvent and metabolite concentration are chosen to facilitate glass formation upon freezing, which supports polarization transfer from the free radical to nearby ^{13}C nuclei. In a polarizer with a 3T field at 1K, electron spins are nearly 100% polarized whereas ^{13}C polarization is on the order of 0.1% (Fig. 2B). Microwave irradiation is used to transfer electron polarization to ^{13}C nuclei, yielding ^{13}C polarization on the order of 10-30%. To remove the hyperpolarized compound from the polarizer, a rapid dissolution is performed in which superheated (>100°C) biological buffer is pumped through the polarizer to melt the hyperpolarized substrate and eject it from the machine. Polarization requires 1-2 hours and the dissolution takes place within a few seconds, yielding upwards of a 10^5-fold increase in spin polarization relative to thermal equilibrium. As a result, high SNR spectra of the hyperpolarized substrate can be acquired in a single scan in under a second. Sequential acquisition of spectra over one to two minutes can be used to monitor the delivery of an intravenously administered hyperpolarized compound to a tumor and to quantify the rate at which it is converted to downstream metabolites. However, the hyperpolarized state is short-lived and each acquisition results in some loss of hyperpolarization, so intelligent data acquisition schemes must be implemented to quickly acquire high SNR data with minimal polarization loss.

DATA ACQUISITION

In magnetic resonance imaging, the raw signal is sampled in the spatial frequency domain, commonly known as k-space, and images are obtained by a Fourier transform of the k-space data. For example, a 3-dimensional volume can be imaged by sampling k-space in 3-dimensions (volumetric imaging) or by acquiring 2-dimensional k-

space datasets for each slice (stack of slices). MRSI builds on these imaging principles by including the time dimension in the sampling scheme to encode both spatial and spectral information. This is commonly accomplished by periodically sampling the same k-space points at an interval corresponding to the spectral resolution. In addition to the periodic oscillations pertaining to spectral information, the time domain data also contain non-periodic signal variations that reflect T_1 relaxation and *in vivo* metabolic activity. Data acquisition regimes that can sample this non-periodic information along the extended time axis can be referred to as dynamic or time-resolved imaging.

Strategies for hyperpolarized ^{13}C imaging must employ a balanced approach that: i) utilizes the non-renewable polarization in an SNR-efficient manner given desired spatial and temporal resolutions, ii) adequately samples the dynamics of the signals of both substrate and metabolites such that metabolic conversion can be monitored, iii) acquires sufficient information to resolve the signals of interest in both spatial and spectral domains, and iv) completes within the lifetime of the signal enhancement.

Spectroscopic Imaging

The most basic implementation of MRSI is chemical shift imaging (CSI) in which a densely sampled set of time domain data (Fig. 3A) is acquired for each point in k-space, allowing reconstruction of a grid of spectra. CSI is robust to off-resonance phenomena such as B_0 inhomogeneity, and the spectral resolution and bandwidth can be easily adjusted by controlling the temporal density of samples and the duration of the readout. However, CSI employs the most time-inefficient spatial encoding scheme because each single line in k vs. t is sampled with a separate radiofrequency excitation and readout (red lines in Fig. 3A). The simultaneous spectral and spatial encoding

presents a trade-off between spectral bandwidth and spatial resolution *(9)*. The number of excitations required by CSI to give the desired spatial coverage and resolution scales with the number of voxels, and this potentially large number of excitations makes the temporal resolution of CSI a limiting factor for hyperpolarized studies.

More efficient k-space sampling can be achieved by using time-varying gradients during each readout interval. For example, echo-planar spectroscopic imaging (Fig. 3B) has been used to encode entire planes of k vs. t per excitation *(10)*. The k-space trajectory is traversed periodically to sample the time dimension. The first-in-human clinical study with hyperpolarized pyruvate in prostate cancer patients utilized echo-planar spectroscopic imaging in both a single time-point mode and a time-resolved mode with 2D spatial encoding *(11)*. Achieving 3D spatial encoding with CSI requires acceleration strategies such as using randomized data undersampling schemes (Fig. 3C) that enable reconstruction of an extended field-of-view (and spectral bandwidth) within the same data sampling time *(12)*.

Fast Imaging

It is typically known *a priori* which metabolites can arise from a given substrate (e.g. pyruvate-hydrate, lactate, alanine and bicarbonate are downstream from 1-^{13}C-pyruvate). Using this, the number of required measurements can be greatly reduced by exploiting this prior knowledge of the metabolites' unique frequencies.

The well known spectral selectivity of steady-state free precession pulse trains in the limit of low flip angles can be exploited to excite one resonance at a time. Although a true steady state is not achievable in the hyperpolarized regime, a pseudo steady state transverse magnetization can be established and sampled across multiple readout

periods in an SNR efficient manner *(13)*. However, the steady-state free precession excitation bandwidths may be narrower than *in vivo* linewidths due to B_0 inhomogeneity such that acquisitions from multiple pulse trains, offset in frequency, must be combined *(14)* to achieve sufficient spectral coverage at the expense of temporal resolution. Higher temporal resolution can be achieved with compressed sensing acceleration *(15)*.

Prior knowledge of the expected relative signal intensities can also be exploited to design spectrally-selective radiofrequency pulses that excite the substrate with a small flip angle (to preserve magnetization) while exciting downstream metabolites with a larger flip angle to facilitate detection *(16)*. This approach can be combined with spectral-decomposition methods to reduce the number of involved species *N (17)*. Spectral-decomposition reconstruction techniques *(18)* are capable of resolving *N* species from *N+1* images by acquiring a data set with incrementally time shifted data acquisitions (Fig. 4E). The measured data are fit to a numerical model of the frequency-dependent phase evolution for each metabolite, resulting in separate images of each species.

Taken further, spectral-spatial radiofrequency pulses (Fig. 4A) can be used to excite a single resonance at a time within a specific spatial extent (Fig. 4B), which is then conventionally encoded by a rapid k-space encoding scheme such as flyback *(19)* (Fig. 4C), dual-echo (Fig. 4D), and symmetric echo-planar *(20,21)* or single-shot spiral *(22,23)* (Fig. 4E) trajectories. In this way, the task of spectral separation is performed before the raw signal is digitized, greatly simplifying the image reconstruction and enabling improved spatial coverage and resolution. For example, polarized pyruvate, the lactate produced in tumor tissue, and a co-polarized perfusion agent were each imaged over a 3D (6 x 8 x 64 cm) field of view with 5 mm spatial resolution and 5 second temporal resolution *(24)*. An alternative to spectral-spatial excitation involves spectrally-

selective pulses with a surface receive coil such that the extent of required spatial encoding is limited by the coil sensitivity profile *(25)*.

HYPERPOLARIZED ^{13}C MRSI PROBES

Probe Design & T_1 Relaxation

Due to the low natural abundance of ^{13}C, the use of ^{13}C-enriched probes can increase the magnetic resonance signal by 100-fold. However, ^{13}C labeling at all carbon positions can be challenging and expensive, so a majority of hyperpolarized probes are labeled at a single site (Fig. 5). One factor to consider when selecting the site of ^{13}C labeling is the chemical shift difference between the substrate and the product at the labeled position. Consider the case of hyperpolarized 1-^{13}C-pyruvate as a lactate dehydrogenase probe, which is the most extensively studied *in vivo* hyperpolarized probe to date. This enzyme catalyzes the conversion of 1-^{13}C-pyruvate to 1-^{13}C-lactate, and the chemical shift at the labeled position for each compound is 171 and 183 parts per million, respectively. Due to this relatively large difference in chemical shift, the peaks for the substrate and product of this enzymatic reaction can be easily resolved and accurate enzymatic flux measurements can be made with MRSI.

Another factor that must be considered when selecting the ^{13}C-labeling site is the T_1 value, also known as the longitudinal relaxation time constant, at that position. Once removed from the polarizer, the hyperpolarized substrate will exponentially relax towards thermal equilibrium polarization. Relative to the polarization at initial time t_0, the T_1 value refers to the amount of time required for the polarization to decay to 1/e (0.368) times that of polarization at t_0. T_1 values are typically on the order of tens of seconds in clinical magnetic resonance imaging field strengths, with the total hyperpolarized signal lifetime

on the order of a few minutes *(26)*. For *in vivo* MRSI applications, longer T_1 times facilitate more accurate quantification of metabolic flux since several time-consuming steps must take place prior to enzymatic conversion of the hyperpolarized substrate at the target tissue. Following dissolution, the sample must be loaded into a syringe, injected intravenously into a patient, the hyperpolarized compound must accumulate in the target tissue, and cells at the target tissue must take up the hyperpolarized compound via membrane transporters before any enzymatic reaction can be measured. During this time, the hyperpolarized substrate is relaxing as a function of its T_1. Carbon atoms that do not have directly attached protons, such as carbonyl groups, tend to have larger T_1 values and a majority of the probes listed in Figure 5 are labeled at these positions. If labeling at a position with directly attached protons is desired, substituting these protons with deuterium can increase T_1 values. Directly attached ^{14}N (99.6% natural abundance) also reduces T_1 values, which can be increased via ^{15}N substitution *(27)*.

Warburg Effect

A majority of hyperpolarized MRSI cancer research has focused on the Warburg Effect, in which cancer cells exhibit elevated levels of glycolysis and lactic acid fermentation. Lactate dehydrogenase mediated conversion of pyruvate to lactate is elevated in malignant cells as a result of the Warburg Effect, and hyperpolarized 1-^{13}C-pyruvate can be used to quantify flux through this pathway. It is currently the only hyperpolarized probe translated to humans, with a first-in-human safety study conducted on prostate cancer patients with untreated, biopsy-proven localized prostate cancer in 2013 *(11)*. Elevated conversion of 1-^{13}C-pyruvate to 1-^{13}C-lactate was detected via ^{13}C

MRSI at primary tumor sites, relative to adjacent normal prostate tissue (Fig. 2C). In some patients, this modality detected elevated 1-^{13}C-lactate levels at sites where conventional magnetic resonance imaging methodologies did not detect anatomic abnormalities, which were later identified as malignant via biopsy. These results highlight the potential of advanced imaging techniques towards improving our ability to detect cancer, and further studies with larger patient cohorts spanning a range of cancer subtypes are currently ongoing.

$^{13}C_6$,1,2,3,4,5,6,6-$^{2}H_7$-glucose has also been studied as an imaging agent in pre-clinical cancer models *(28)*. Glucose is metabolically upstream of pyruvate, which allows for the detection of glycolytic intermediates and pentose phosphate pathway metabolites in addition to lactate dehydrogenase-mediated lactate production. In addition, the plasma concentration of glucose is significantly higher than that of pyruvate, which allows the imaging dose of hyperpolarized $^{13}C_6$,1,2,3,4,5,6,6-$^{2}H_7$-glucose to fall closer to physiological concentrations when compared to hyperpolarized 1-^{13}C-pyruvate. These factors may indicate that the data from hyperpolarized glucose is more biologically relevant, but the significantly shorter T_1 values of all glucose carbons relative to the carboxyl carbon of pyruvate makes accurate *in vivo* quantification and human translation of hyperpolarized glucose difficult.

Glutaminolysis

In addition to glycolysis, cancer cells undergo glutaminolysis, the uptake and metabolism of glutamine, to meet their high energetic demands. Glutamine is metabolized to the tricarboxylic acid cycle intermediate α-ketoglutarate, and it can be further metabolized to pyruvate with concomitant production of NADH/NADPH, supplying

the cell with reducing equivalents to support biosynthesis. The first step into this pathway is mediated by an amidohydrolase (e.g. glutaminase), which catalyzes the conversion of glutamine to glutamate. An *in vitro* study with hyperpolarized 5-^{13}C,4-$^{2}H_2$-glutamine in SF188-Bcl-x_L human glioma cells revealed that glutaminase-mediated glutamate production can be detected in real time via nuclear magnetic resonance *(29)*. The study also found glutamine uptake outpaced that of 2-^{18}F-fluoro-2-deoxyglucose in their glioma model, suggesting hyperpolarized 5-^{13}C,4-$^{2}H_2$-glutamine may be more cancer-specific than 2-^{18}F-fluoro-2-deoxyglucose *in some cases.*

IDH Mutation

Along with up- or down-regulation of existing metabolic pathways, cancer cells can exhibit mutations in which new enzymatic pathways are created. IDH normally catalyzes the decarboxylation of isocitrate to α-ketoglutarate, but some cancer subtypes acquire an IDH mutation that results in the gain of a novel function. IDH mutations can be found in gliomas, and the mutant enzyme catalyzes the conversion of α- ketoglutarate to 2-hydroxyglutarate. Hyperpolarized 1-^{13}C-α-ketoglutarate has been used for ^{13}C-MRSI in a pre-clinical murine orthotopic U87 glioblastoma model and showed potential to differentiate IDH1 mutant and wildtype tumors *(30)*. Since IDH inhibitors are used to treat certain gliomas, non-invasive assessment of IDH mutational status would be valuable towards guiding therapy selection and monitoring therapy response.

Reactive Oxygen Species and Redox Chemistry

Elevated levels of reactive oxygen species are associated with a variety of pathologies such as cancer, and its etiologies range from elevated metabolism to

mitochondrial dysfunction. To protect the cell from oxidative stress, cancer cells upregulate intracellular levels of the antioxidant glutathione. Increased reduction of 1-^{13}C-dehydroscorbate to 1-^{13}C-vitamin C is an indicator of high glutathione concentrations, which can be associated with malignancy. ^{13}C-MRSI with hyperpolarized 1-^{13}C-dehydroscorbate in a transgenic adenocarcinoma of the mouse prostate model revealed high 1-^{13}C-vitamin C in the liver, kidney, and prostate tumor *(31)*. Moreover, the rodent brain demonstrated high rates of dehydroscorbate reduction to vitamin C, highlighting the reductive capacity of the brain. Increased dehydroscorbate reduction in the liver is due to high levels of glutathione-mediated detoxification that regularly occurs in this tissue, whereas elevated vitamin C in the tumor is the result of an adaptive change against increased oxidative stress within cancer cells.

pH

Augmented metabolism and active secretion of protons by tumor cells support an acidic tumor microenvironment, which can reduce the local pH to ~6.5, as compared to pH ~7.4 in healthy tissue. An accurate measurement of tumor pH can help guide treatment plans and determine prognosis, as lower tumor pH is associated with increased likelihood of metastasis and chemotherapeutic resistance. To accurately measure pH in this range, a hyperpolarized pH probe must exhibit a pK_a within this pH window and should be ^{13}C labeled at a site close to the site of the exchanging proton. Close proximity to the exchangeable proton influences the chemical shift at the labeled ^{13}C position to change with pH, with the dynamic range governed by the Henderson-Hasselbalch equation and typically residing between 1 pH unit below and above the pK_a value. Therefore, a titration curve of pH versus chemical shift can be generated across

this range and used as a reference to measure pH *in vivo*, but finding a compound that meet these requirements with a long T_1 value has proven to be challenging. In a pre-clinical ^{13}C-MRSI study with hyperpolarized N-2-^{13}C,2-^{15}N-acetamido-2-aminoethanesulfonic acid (pK_a = 6.56), water phantoms of known pH between 6.47 – 7.44 were used to test the ability of this probe to measure pH *(32)*. The calculated pH values with the hyperpolarized probe were relatively accurate, typically 0.1 – 0.2 pH units off from the measured pH of the solutions. Further studies and translation are required to determine if this level of error can be tolerated while providing clinically relevant information, and new hyperpolarized probes with a pK_a closer to 6.9 or improved data acquisition methods will be required to reduce the magnitude of this error.

CONCLUSION

The first-in-human trial with hyperpolarized 1-^{13}C-pyruvate revealed that pyruvate-to-lactate conversion can be non-invasively detected in the tumor of a patient, and this advanced imaging technique has the potential to identify disease at sites not routinely detected by today's conventional imaging techniques. However, cancer cells undergo a host of other recently characterized metabolic aberrations. Numerous groups are working towards developing hyperpolarized probes that target these alternate pathways, while others focus on improving data acquisition and image reconstruction methods. As these fields of hyperpolarized research progress, additional hyperpolarized probes can be translated to human studies. Meanwhile, expanding current clinical research in the setting of hyperpolarized 1-^{13}C-pyruvate will be instrumental in determining the role this imaging modality will play in cancer care.

REFERENCES

1. Pavlova NN, Thompson CB. The emerging hallmarks of cancer metabolism. *Cell Metab*. 2016;23:27-47.
2. Deberardinis RJ, Chandel NS. Fundamentals of cancer metabolism. *Sci Adv*. 2016;2.
3. Groheux D, Espié M, Giacchetti S, Hindié E. Performance of FDG PET/CT in the clinical management of breast cancer. *Radiology*. 2013;266:388-405.
4. Bobrovnikova-Marjon E, Hurov JB. Targeting metabolic changes in cancer: novel therapeutic approaches. *Annu Rev Med*. 2014;65:157-170.
5. Vander Heiden MG. Targeting cancer metabolism: a therapeutic window opens. *Nat Rev Drug Discov*. 2011;10:671-684.
6. Tee S-S, Keshari KR. Novel approaches to imaging tumor metabolism. *Cancer J*. 2015;21:165-173.
7. Hansson G. Generating highly polarized nuclear spins in solution using dynamic nuclear polarization. *Nucl Instruments Methods Phys Res A*. 2004;526:173-181.
8. Comment A, Merritt ME. Hyperpolarized magnetic resonance as a sensitive detector of metabolic function. *Biochemistry*. 2014;53:7333-7357.
9. Josan S, Hurd R, Park JM, et al. Dynamic metabolic imaging of hyperpolarized [2-13C]pyruvate using spiral chemical shift imaging with alternating spectral band excitation. *Magn Reson Med*. 2014;71:2051-2058.
10. Durst M, Koellisch U, Frank A, et al. Comparison of acquisition schemes for hyperpolarised 13C imaging. *NMR Biomed*. 2015;28:715-725.
11. Nelson SJ, Kurhanewicz J, Vigneron DB, et al. Metabolic imaging of patients with prostate cancer using hyperpolarized [1-^{13}C]pyruvate. *Sci Transl Med*. 2013;5:198ra108.
12. Wang JX, Merritt ME, Sherry AD, Malloy CR. Accelerated chemical shift imaging of hyperpolarized 13C metabolites. *Magn Reson Med*. 2016;76:1033-1038.
13. Shang H, Sukumar S, von Morze C, et al. Spectrally selective three-dimensional dynamic balanced steady-state free precession for hyperpolarized C-13 metabolic imaging with

spectrally selective radiofrequency pulses. *Magn Reson Med*. 2016 [Epub ahead of print].

14. von Morze C, Sukumar S, Reed GD, et al. Frequency-specific SSFP for hyperpolarized 13C metabolic imaging at 14.1 T. *Magn Reson Imaging*. 2013;31:163-170.
15. Milshteyn E, von Morze C, Reed GD, et al. Development of high resolution 3D hyperpolarized carbon-13 MR molecular imaging techniques. *Magn Reson Imaging*. 2017;38:152-162.
16. Schulte RF, Sperl JI, Weidl E, et al. Saturation-recovery metabolic-exchange rate imaging with hyperpolarized [1-13C] pyruvate using spectral-spatial excitation. *Magn Reson Med*. 2013;69:1209-1216.
17. Sigfridsson A, Weiss K, Wissmann L, et al. Hybrid multiband excitation multiecho acquisition for hyperpolarized ^{13}C spectroscopic imaging. *Magn Reson Med*. 2015;73:1713-1717.
18. Wiesinger F, Weidl E, Menzel MI, et al. IDEAL spiral CSI for dynamic metabolic MR imaging of hyperpolarized [1- 13C]pyruvate. *Magn Reson Med*. 2012;68:8-16.
19. Cunningham CH, Dominguez Viqueira W, Hurd RE, Chen AP. Frequency correction method for improved spatial correlation of hyperpolarized 13C metabolites and anatomy. *NMR Biomed*. 2014;27:212-218.
20. Gordon JW, Vigneron DB, Larson PEZ. Development of a symmetric echo planar imaging framework for clinical translation of rapid dynamic hyperpolarized 13C imaging. *Magn Reson Med*. 2016;832:826-832.
21. Miller JJ, Lau AZ, Teh I, et al. Robust and high resolution hyperpolarized metabolic imaging of the rat heart at 7T with 3D spectral-spatial EPI. *Magn Reson Med*. 2016;75:1515-1524.
22. Durst M, Koellisch U, Daniele V, et al. Probing lactate secretion in tumours with hyperpolarised NMR. *NMR Biomed*. 2016;29:1079-1087.
23. Wang J, Wright AJ, Hu D en, Hesketh R, Brindle KM. Single shot three-dimensional pulse sequence for hyperpolarized 13C MRI. *Magn Reson Med*. 2016;752:740-752.

24. Lau JYC, Chen AP, Gu YP, Cunningham CH. Voxel-by-voxel correlations of perfusion, substrate, and metabolite signals in dynamic hyperpolarized 13C imaging. *NMR Biomed*. 2016;29:1038-1047.

25. Lau AZ, Miller JJ, Tyler DJ. Mapping of intracellular pH in the in vivo rodent heart using hyperpolarized [1-13C]pyruvate. *Magn Reson Med*. 2017;77:1810-1817.

26. Keshari KR, Wilson DM. Chemistry and biochemistry of 13C hyperpolarized magnetic resonance using dynamic nuclear polarization. *Chem Soc Rev*. 2014;43:1627-1659.

27. Chiavazza E, Kubala E, Gringeri C V., et al. Earth's magnetic field enabled scalar coupling relaxation of 13C nuclei bound to fast-relaxing quadrupolar 14N in amide groups. *J Magn Reson*. 2013;227:35-38.

28. Rodrigues TB, Serrao EM, Kennedy BWC, Hu D-E, Kettunen MI, Brindle KM. Magnetic resonance imaging of tumor glycolysis using hyperpolarized 13C-labeled glucose. *Nat Med*. 2014;20:93-97.

29. Qu W, Zha Z, Lieberman BP, et al. Facile synthesis [5-(13)C-4-(2)H(2)]-L-glutamine for hyperpolarized MRS imaging of cancer cell metabolism. *Acad Radiol*. 2011;18:932-939.

30. Chaumeil MM, Larson PEZ, Yoshihara H a I, et al. Non-invasive in vivo assessment of IDH1 mutational status in glioma. *Nat Commun*. 2013;4:2429.

31. Keshari KR, Kurhanewicz J, Bok R, Larson PEZ, Vigneron DB, Wilson DM. Hyperpolarized 13C dehydroascorbate as an endogenous redox sensor for in vivo metabolic imaging. *Proc Natl Acad Sci U S A*. 2011;108:18606-18611.

32. Flavell RR, Morze C Von, Blecha JE, et al. Application of Good's buffers to pH imaging using hyperpolarized 13C MRI. *Chem Commun*. 2015;51:14119-14122.

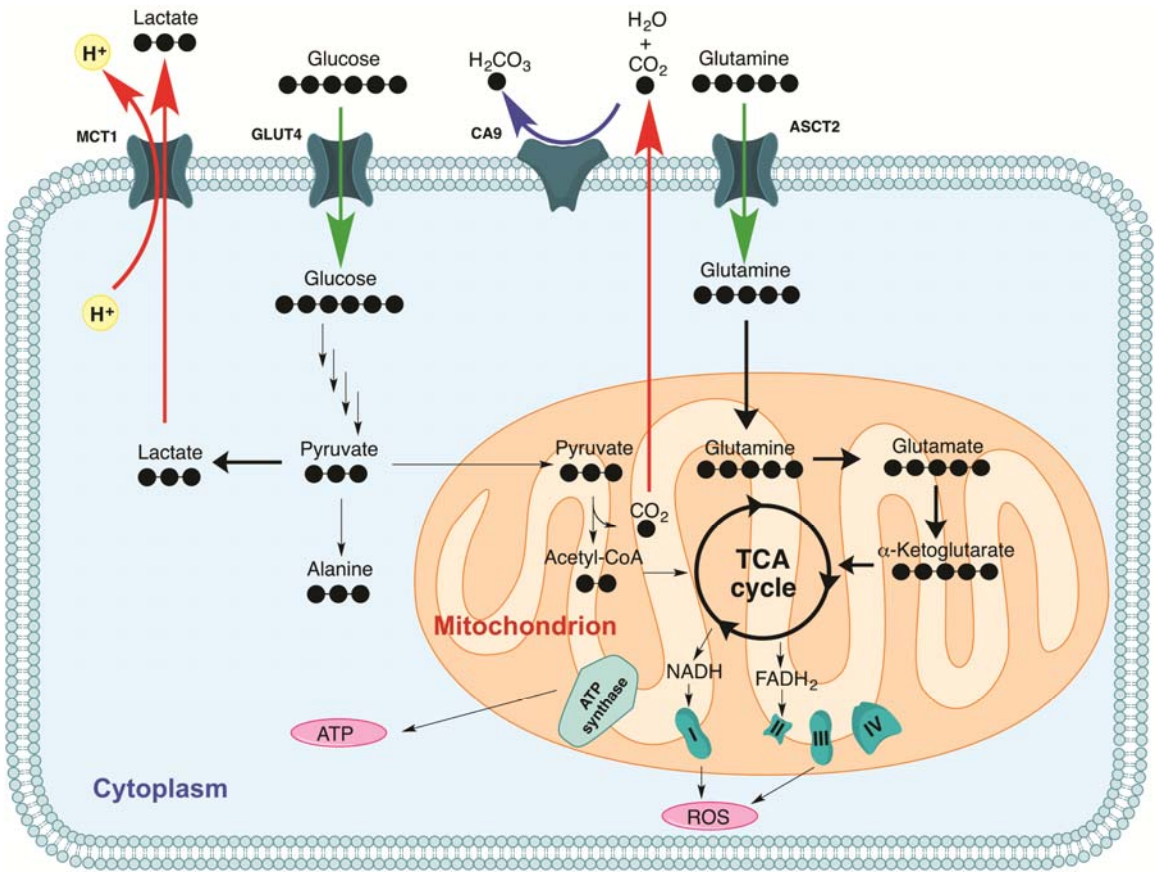

Figure 1. Schematic of metabolic changes in cancer metabolism highlighted in this review. Bold lines indicate up-regulation of this pathway relative to non-malignant cells.

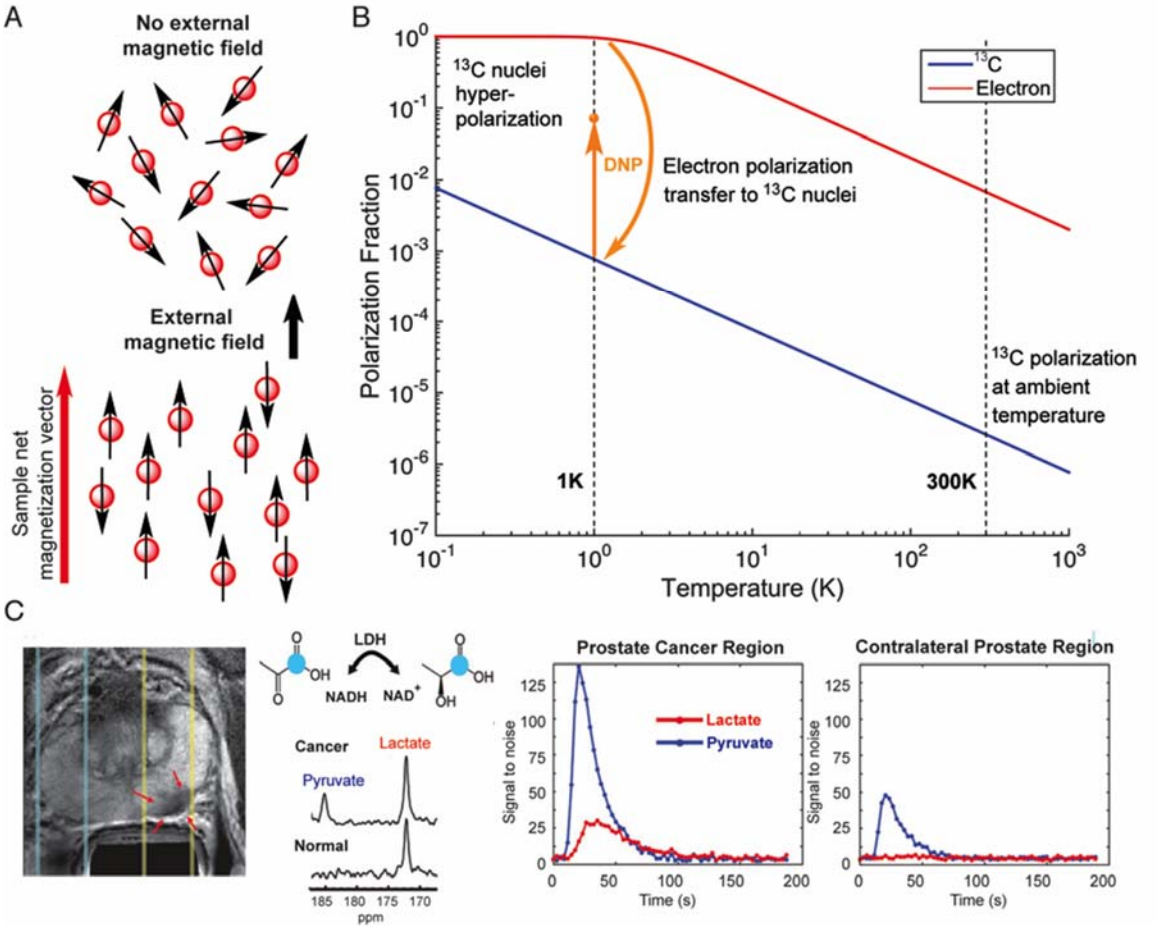

Figure 2. (A) Illustration of alignment of carbon nuclear spins (red balls with arrow) in the absence (top) and presence (bottom) of an external magnetic field. (B) Spin polarization of carbon nuclei and electrons in a 3T magnetic field versus temperature. In dynamic nuclear polarization, electron spin polarization is transferred to carbon nuclei via microwave irradiation. (C) (left to right) Axial T_2-weighted image of a prostate, with the red arrows indicating a region of biopsy-proven cancer. The spectra in the next panel were collected at the region containing the tumor (indicated by yellow lines) or contralateral healthy prostate (indicated by light blue lines) 36 seconds following intravenous injection of hyperpolarized 1-^{13}C-pyruvate. The spectrum from the cancer region contains a prominent lactate peak due to the Warburg effect. The two plots on the right show the hyperpolarized pyruvate and lactate signal as a function of time at the prostate cancer and contralateral regions. The accumulation and hyperpolarized signal decay of pyruvate is seen in both regions, but conversion to lactate and subsequent lactate signal decay is only observed in the prostate cancer region.

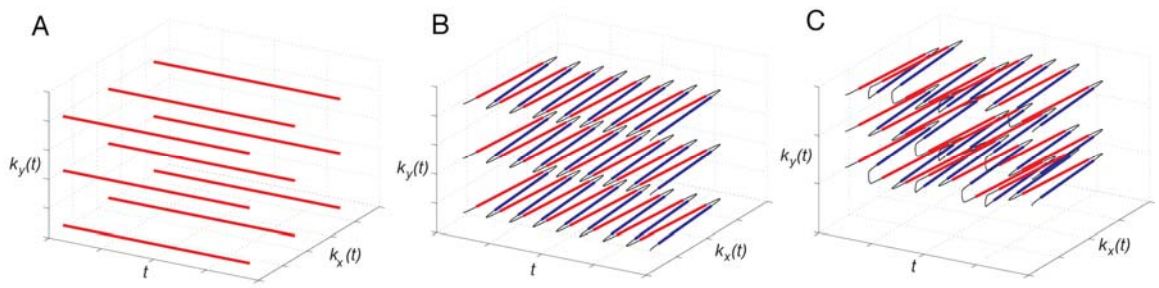

Figure 3. Data sampling distributions for chemical-shift imaging acquisition methods. (A) Conventional chemical-shift imaging offers excellent spectral quality, with dense sampling along the time axis, but each read line requires a separate radiofrequency excitation and sampling period and is consequently slow. Echo-planar spectroscopic imaging (B) enables sampling of an entire plane of the data space upon each excitation (the planes visible in (B)). A sampling pattern that contains random jumps between k-t planes (C) enables extended spatial coverage and spectral bandwidth within the same sampling time.

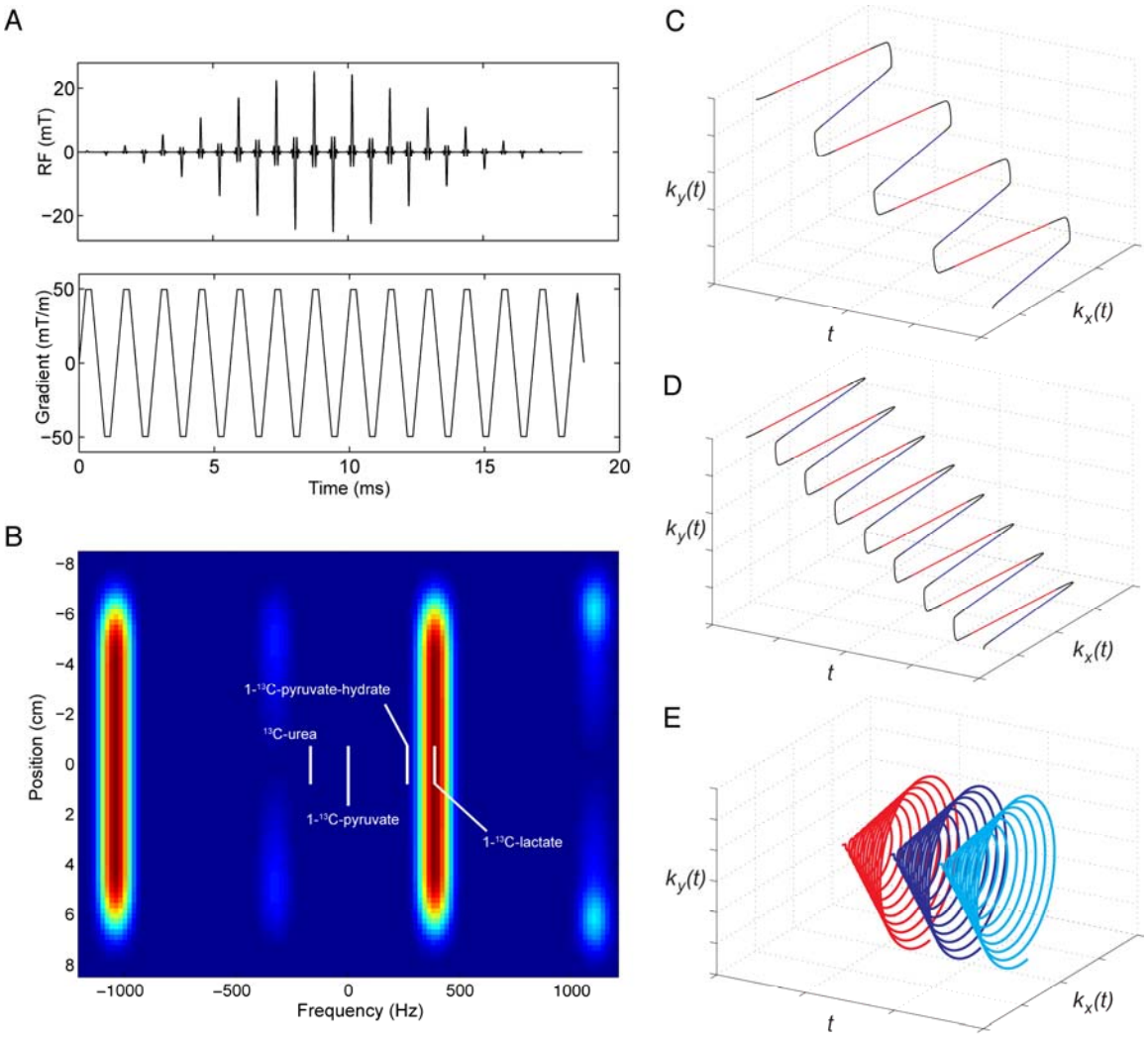

Figure 4. Spectral-spatial excitation and the rapid imaging trajectories that are enabled. Spectral-spatial pulses (A) consist of repeated RF sublobes, played in the presence of an oscillating gradient waveform. The excitation profile of such a pulse (B) excites "islands" of magnetization that can be placed on the spectral components of interest. Conventional fast-imaging acquisitions such as (C) echo-planar imaging and (D) dual-echo echo-planar imaging are enabled when single resonances are excited. Imaging data acquired at successive time shifts (E) enables separation of signal from multiple resonances, such as the pyruvate-hydrate signal that may contaminate the lactate image.

Name	Structure
1-^{13}C-Pyruvate	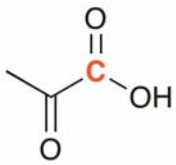
$^{13}C_6$,1,2,3,4,5,6,6-$^{2}H_7$-Glucose	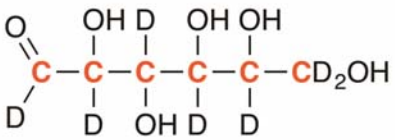
4-$^{2}H_2$,5-^{13}C-Glutamine	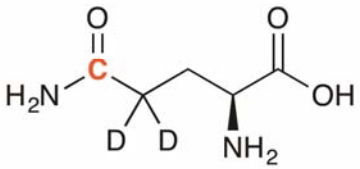
1-^{13}C-α-Ketoglutarate	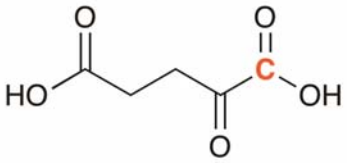
1-^{13}C-Dehydroascorbate	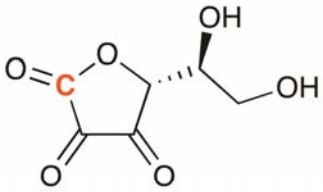
N-(2-^{13}C,2-^{15}N-2-Acetamido)-2-Aminoethanesulfonic Acid	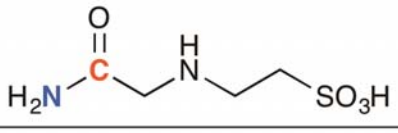

 Carbon-13  Nitrogen-15

Figure 5. Names and structures of hyperpolarized ^{13}C-MRSI probes featured in this review.